

# Relativistic Radiative and Auger Rates for Fe xxIV

M. A. Bautista

*Centro de Física, IVIC, Caracas 1020A, Venezuela*

C. Mendoza<sup>1</sup>, T. R. Kallman, and P. Palmeri<sup>2</sup>

*NASA Goddard Space Flight Center, Greenbelt, MD 20771*

## ABSTRACT

As part of a project to compute improved atomic data for the spectral modeling of iron K lines, we report extensive calculations and comparisons of radiative and Auger rates for transitions involving the K-vacancy states in Fe xxIV. By making use of several computational codes, a detailed study is carried out of orbital representations, configuration interaction, relativistic corrections, cancellation effects, and fine tuning. It is shown that a formal treatment of the Breit interaction is essential to render the important magnetic correlations that take part in the decay pathways of this ion. As a result, the accuracy of the present  $A$ -values is firmly ranked at better than 10% while that of the Auger rates at only 15%.

*Subject headings:* atomic data – atomic processes – line formation – X-rays: spectroscopy

## 1. Introduction

Iron K lines are among the most interesting features in astronomical X-ray spectra. These lines appear in many cosmic X-ray sources, they are located in a relatively unconfused spectral region, and have a well understood potential in plasma diagnostics. Detections date to the earliest rocket experiments on astronomical X-ray spectra (Chubb et al. 1963; Serlemitsos et al. 1973). Iron K line observations have helped to determine flare temperatures in the Sun (Doschek et al. 1981) and supernova remnants (Serlemitsos et al. 1973), the

---

<sup>1</sup>Permanent address: Centro de Física, IVIC, Caracas 1020A

<sup>2</sup>Research Associate at Department of Astronomy, University of Maryland, College Park, MD 20742

emission geometry in X-ray binaries (Sanford et al. 1975; Pravdo et al. 1977), have revealed the presence of extragalactic nuclear processed material in clusters of galaxies (Serlemitsos et al. 1977), and strong gravity in Seyfert galaxies (Tanaka et al. 1995).

Recent improvements in the spectral capabilities and sensitivity of satellite-borne X-ray telescopes (*Chandra*, *XMM-Newton*) have promoted the role of Fe K lines in diagnostics, trend that will continue to evolve with the launch of future instruments such as *Astro-E2* and *Constellation-X*. Plasma diagnostics such as those devised from the iron K spectrum ultimately rely on the knowledge of the microphysics of line formation and hence on the accuracy of the atomic data. In spite of the line identifications by Seely et al. (1986) in solar flare spectra and the laboratory measurements of Beiersdorfer et al. (1989, 1993), Decaux & Beiersdorfer (1993) and Decaux et al. (1995, 1997), the K-vacancy level structures of Fe ions remain incomplete as can be concluded from the recent critical compilation of Shirai et al. (2000). With regards to radiative and Auger rates, the highly ionized members of the isonuclear sequence, namely Fe xxv–Fe xxI, have received much attention, and the comparisons by Chen (1986) and Kato et al. (1997) have brought about some degree of data assurance. For Fe ions with an electron occupancy greater than 9, Jacobs et al. (1980) and Jacobs and Rosznyai (1986) have carried out central field calculations on the structure and widths of various inner-shell transitions, but these have not been subject to independent checks and do not suffice current requirements of level-to-level data.

The present report is the first in a project to systematically compute improved atomic data sets for the modeling of K spectra. The emphasis is both on accuracy and completeness. For this purpose, we make use of several state-of-the-art atomic physics codes to deliver for the Fe isonuclear sequence: energy levels; wavelengths; radiative, Auger and electron impact excitation rates; and photoionization cross sections. In the case of Fe xxIV, transitions of the type  $1s^2 nl - 1s2pnl$  with  $n \geq 2$  yield satellite lines on the red wing of the  $1s^2 - 1s2p$  lines of helium-like Fe xxV at  $1.85\text{\AA}$ . These satellite lines blend with the Fe xxV emission lines in low and medium resolution spectra and distort the observed emission line ratios often used in plasma diagnostics (Bautista & Kallman 2000; Oelgoetz & Pradhan 2001). We have approached the radiative and autoionization (Auger) properties of Fe xxIV as a test case of the numerical methods and of the relevance of the different physical effects. By detailed comparisons with previous work, it has become evident that there is room for improvement, that some of the computational packages are deficient for the study of K-shell processes, and that an efficient strategy can be prescribed for the treatment of the whole sequence.

## 2. Numerical methods

In the present work we employ three different computational packages to study the decay properties of the  $n = 2$  K-vacancy states of Li-like Fe XXIV.

**AUTOSTRUCTURE:** an extension by Badnell (1986, 1997) of the atomic structure code SUPERSTRUCTURE (Eissner et al. 1974) to treat autoionization processes. It also integrates piecemeal developments that have been carried out over the years to implement improvements in the relativistic framework, term-energy corrections, and Coulomb–Born high-energy limits.

**HFR:** the Hartree–Fock suite of codes by Cowan (1981) that includes relativistic corrections. It is used to calculate level energies, wavelengths, oscillator strengths, and in a perturbation approach, autoionization rates.

**BPRM:** the Breit–Pauli version of the R-matrix electron scattering code (Burke et al. 1971; Berrington et al. 1974, 1978, 1987; Scott & Burke 1980; Scott & Taylor 1982). Resonance parameters are computed in the asymptotic region with the STGQB module by Quigley & Berrington (1996) and Quigley et al. (1998).

We have found the Fe Li-like system to be an unusually versatile workbench for the magnetic interactions, a fact that perhaps has not been always appreciated in previous work. Thus prior to the description of the numerical details of the codes, we include a concise summary of the relativistic Breit–Pauli Hamiltonian which is used throughout our computational portfolio and will be central in the discussion of results.

### 2.1. Breit–Pauli Hamiltonian

The Breit–Pauli Hamiltonian for an  $N$ -electron system is given by

$$H_{\text{bp}} = H_{\text{nr}} + H_{1\text{b}} + H_{2\text{b}} \quad (1)$$

where  $H_{\text{nr}}$  is the usual non-relativistic Hamiltonian. The one-body relativistic operators

$$H_{1\text{b}} = \sum_{n=1}^N f_n(\text{mass}) + f_n(\text{d}) + f_n(\text{so}) \quad (2)$$

represent the spin–orbit interaction,  $f_n(\text{so})$ , and the non-fine structure mass-variation,  $f_n(\text{mass})$ , and one-body Darwin,  $f_n(\text{d})$ , corrections. The two-body corrections

$$H_{2\text{b}} = \sum_{n>m} g_{nm}(\text{so}) + g_{nm}(\text{ss}) + g_{nm}(\text{css}) + g_{nm}(\text{d}) + g_{nm}(\text{oo}) , \quad (3)$$

usually referred to as the Breit interaction, include, on the one hand, the fine structure terms  $g_{nm}(\text{so})$  (spin-other-orbit and mutual spin-orbit) and  $g_{nm}(\text{ss})$  (spin-spin), and on the other, the non-fine structure terms:  $g_{nm}(\text{css})$  (spin-spin contact),  $g_{nm}(\text{d})$  (two-body Darwin), and  $g_{nm}(\text{oo})$  (orbit-orbit).

The radiative rates ( $A$ -values) for electric dipole and quadrupole transitions are respectively given in units of  $\text{s}^{-1}$  by the expressions

$$A_{\text{E}1}(k, i) = 2.6774 \times 10^9 (E_k - E_i)^3 \frac{1}{g_k} S_{\text{E}1}(k, i) \quad (4)$$

$$A_{\text{E}2}(k, i) = 2.6733 \times 10^3 (E_k - E_i)^5 \frac{1}{g_k} S_{\text{E}2}(k, i) \quad (5)$$

where  $S(k, i)$  is the line strength,  $g_k$  the statistical weight of the upper level, with energies given in Rydberg units and lengths in Bohr radii. Similarly for magnetic dipole and quadrupole transitions, the  $A$ -values are

$$A_{\text{M}1}(k, i) = 3.5644 \times 10^4 (E_k - E_i)^3 \frac{1}{g_k} S_{\text{M}1}(k, i) \quad (6)$$

$$A_{\text{M}2}(k, i) = 2.3727 \times 10^{-2} (E_k - E_i)^5 \frac{1}{g_k} S_{\text{M}2}(k, i) . \quad (7)$$

Due to the strong magnetic interactions in this ion, the magnetic dipole line strength is assumed to take the form

$$S_{\text{M}1}(k, i) = |\langle k | \mathbf{P} | i \rangle|^2 \quad (8)$$

where

$$\mathbf{P} = \mathbf{P}^0 + \mathbf{P}^1 = \sum_{n=1}^N \{ \mathbf{l}(n) + \boldsymbol{\sigma}(n) \} + \mathbf{P}^{\text{rc}} . \quad (9)$$

$\mathbf{P}^0$  is the usual low-order M1 operator and  $\mathbf{P}^{\text{rc}}$  includes the relativistic corrections established by Drake (1971). Although the main astrophysical interest is in E1  $\text{K}\alpha$  decays, it is shown here that some of the forbidden transitions display  $A$ -values comparable with the E1 type and therefore must be taken into account for accuracy. Furthermore, in the case of the  $1s2s2p\ ^4\text{P}_{5/2}^0$  state, radiative decay can only occur through forbidden transitions.

## 2.2. AUTOSTRUCTURE

AUTOSTRUCTURE (Badnell 1986, 1997), an extension of the atomic structure program SUPERSTRUCTURE (Eissner et al. 1974), computes fine structure level energies and radiative and Auger rates in a Breit–Pauli relativistic framework. Single electron orbitals,  $P_{nl}(r)$ , are constructed by diagonalizing the non-relativistic Hamiltonian,  $H_{nr}$ , with a statistical Thomas–Fermi–Dirac model potential  $V(\lambda_{nl})$  (Eissner & Nussbaumer 1969). The  $\lambda_{nl}$  scaling parameters are optimized variationally by minimizing a weighted sum of the  $LS$  term energies. The latter are represented by configuration-interaction (CI) wavefunctions of the type

$$\Psi = \sum_i c_i \phi_i . \quad (10)$$

Continuum wavefunctions are constructed within the distorted-wave approximation. Relativistic fine structure levels and rates are obtained by diagonalizing the Breit–Pauli Hamiltonian in intermediate coupling. Both one- and two-body operators—fine structure and non-fine structure (see Section 2.1)—have been fully implemented to order  $\alpha^2 Z^4$  where  $\alpha$  is the fine structure constant and  $Z$  the atomic number. The relativistic corrections to the M1 operator (see Eq. 9) have been incorporated in SUPERSTRUCTURE by Eissner & Zeippen (1981).

Fine tuning—which is advisable for treating states that decay through weak relativistic couplings (e.g. intercombination transitions)—is managed by means of term energy corrections (TEC). By considering the relativistic wavefunction,  $\psi_i^r$ , in a perturbation expansion in terms of the non-relativistic functions  $\psi_i^{\text{nr}}$ ,

$$\psi_i^r = \psi_i^{\text{nr}} + \sum_{j \neq i} \psi_j^{\text{nr}} \times \frac{\langle \psi_j^{\text{nr}} | H_{1b} + H_{2b} | \psi_i^{\text{nr}} \rangle}{E_i^{\text{nr}} - E_j^{\text{nr}}} , \quad (11)$$

a modified  $H_{nr}$  is constructed with improved estimates of the differences  $E_i^{\text{nr}} - E_j^{\text{nr}}$  so as to adjust the centers of gravity of the spectral multiplets to the experimental values. This procedure therefore relies on the availability of spectroscopic data.

## 2.3. HFR

In the HFR code by Cowan (1981), an orbital basis is obtained for each electronic configuration by solving the Hartree–Fock equations for the spherically averaged atom. The equations result from the application of the variational principle to the configuration average energy and include relativistic corrections, namely the Blume–Watson spin–orbit, mass–

velocity and one-body Darwin terms. The Blume–Watson spin–orbit term comprises the part of the Breit interaction that can be reduced to a one-body operator.

The multiconfiguration Hamiltonian matrix is constructed and diagonalized in the  $LSJ\pi$  representation of the Slater–Condon theory. Each matrix element is a sum of products of Racah angular coefficients and radial integrals (Slater and spin–orbit integrals)

$$\langle a | H | b \rangle = \sum_i c_i^{a,b} I_i^{a,b}. \quad (12)$$

The radial parameters,  $I_i^{a,b}$ , can be adjusted to reproduce the experimental energy levels in a subsequent least-squares fitting procedure. The eigenvalues and eigenstates thus obtained (*ab initio* or semi-empirically) are used to compute the wavelength and oscillator strength for each possible transition.

The autoionization rates are calculated using the perturbation theory expression

$$\begin{aligned} A_a &= \frac{2\pi}{\hbar} V_\varepsilon^2 \\ &= \frac{2\pi}{\hbar} |\langle \alpha LSJ\pi | H | \alpha' L'S'J'\varepsilon l LSJ\pi \rangle|^2. \end{aligned} \quad (13)$$

Here  $\alpha$  embodies the coupling scheme and the remaining quantum numbers necessary to define the initial state;  $\alpha'$  plays a similar role for the threshold state to which the continuum electron,  $\varepsilon l$ , is coupled. The kinetic energy of the free electron,  $\varepsilon$ , is determined as the difference between the average energy of the autoionizing and the threshold configurations. The radial wave functions of the initial and final states are optimized separately. Both states are calculated in intermediate coupling but CI is accounted for only in the autoionizing states, i.e. no interaction between the threshold electronic configurations is assumed. The continuum orbitals,  $P_{\varepsilon l}(r)$ , are solutions of the Hartree-plus-Statistical-Exchange equations for fixed positive values of the  $\varepsilon$  Lagrangian multipliers (Cowan 1981).

## 2.4. BPRM

The BPRM method is widely used in electron–ion scattering and in radiative bound–bound and bound–free calculations. It is based on the close-coupling approximation of Burke & Seaton (1971) whereby the wavefunctions for states of an  $N$ -electron target and a colliding electron with total angular momentum and parity  $J\pi$  are expanded in terms of the target eigenfunctions

$$\Psi^{J\pi} = \mathcal{A} \sum_i \chi_i \frac{F_i(r)}{r} + \sum_j c_j \Phi_j. \quad (14)$$

The functions  $\chi_i$  are vector coupled products of the target eigenfunctions and the angular part of the incident-electron functions,  $F_i(r)$  are the radial part of the latter, and  $\mathcal{A}$  is an antisymmetrization operator. The functions  $\Phi_j$  are bound-type functions of the total system constructed with target orbitals; they are introduced to compensate for orthogonality conditions imposed on the  $F_i(r)$  and to improve short-range correlations. The Kohn variational principle gives rise to a set of coupled integro-differential equations that are solved by R-matrix techniques (Burke et al. 1971; Berrington et al. 1974, 1978, 1987) within a box of radius, say,  $r \leq a$ . In the asymptotic region ( $r > a$ ), resonance positions and widths are obtained from fits of the eigenphase sums with the STGQB module developed by Quigley & Berrington (1996) and Quigley et al. (1998). Normalized partial widths are defined from projections onto the open channels. Breit–Pauli relativistic corrections have been introduced in the R-matrix suite by Scott & Burke (1980) and Scott & Taylor (1982), but the two-body terms (see Eq. 3) have not as yet been taken into account. Inter-channel coupling in the scattering problem is equivalent to CI in atomic structure, and represents a formal and unified approach to study the decay properties of both bound states and resonances.

### 3. Results

Since the present study of the Fe Li-like system has been approached as a test case, the atomic data, namely energy levels, wavelengths,  $A$ -values, and Auger rates, are computed in several approximations and extensively compared with other data sets. This methodology is destined to bring out the dominant physical effects and the flaws and virtues of the different numerical packages. Additionally, it provides statistics for determining accuracy ratings, something which has not been established firmly in the past. Since numerous calculations have been performed, only a representative selection is presented (see key in Table 1).

Three calculations with AUTOSTRUCTURE are listed: AST1, the ion model is represented with configurations solely from the  $n = 2$  complex and excludes the Breit interaction, i.e. the relativistic two-body operators in Eq. (3); AST2, the same as AST1 but includes the Breit interaction; AST3 takes into account the latter, single and double excitations to the  $n = 3$  complex, and TEC. The latter model enables the estimate of CI effects from higher complexes and the fine tuning of the final deliverable data set. Two computations with HFR: HFR1 is equivalent to AST2; in HFR2, full  $n = 3$  CI is included and the radial integrals are fitted to reproduce experimental energies (this approximation should be equivalent to AST3). BPR1 is a computation with BPRM wherein the He-like target is represented with the 7 levels from the  $1s^2$ ,  $1s2s$ , and  $1s2p$  configurations. Since BPRM does not take into account the Breit interaction, BPR1 should be comparable with AST1.

We also compare with five external data sets (see Table 1). COR, corresponds to the data set referred to as “Cornille” in Kato et al. (1997) computed with the program AUTOLSJ (Dubau & Loulergue 1981), an earlier but similar implementation of AUTOSTRUCTURE. SAF contains the data set “Safranova” in Kato et al. (1997) and energy levels reported in Safranova & Shlyaptseva (1996) that have been obtained with a  $1/Z$  perturbation method. This method uses a hydrogenic orbital basis, the correlation energy includes contributions from both discrete and continuum states, and the two-body operators of the Breit interaction and QED effects are obtained in a hydrogenic approximation through screening constants. BPR2 contains both  $A$ -values and Auger widths calculated with BPRM by Nahar et al. (2002) using a target model that comprises levels with  $n > 2$ . HFR3 by Lemen et al. (1984) gives Auger rates computed with HFR in a single configuration approximation (i.e. no CI even within  $n = 2$ ), the Breit interaction is not taken into account, and the Coulomb integrals are empirically scaled by 15% to allow for neglected effects. MCDF (Chen 1986) contains data computed in a multiconfiguration Dirac–Fock model that accounts for the Breit interaction and QED in the transition energy, but excludes the exchange interaction between the bound and continuum electrons.

In the context of the calculations of Auger decays with AUTOSTRUCTURE, a dilemma quickly arises regarding ion representation, whether to use Li-type orbitals (parent ion) or those of the He-like remnant. By comparison with results from the more formal BPRM method, it becomes clear that the latter type is the superior choice. On the other hand, the situation is less certain for the  $K\alpha$  radiative data due to the absence of noticeable differences. In this case, and due to somewhat better agreement with previous work, the  $A$ -values have been calculated with parent orbitals.

### 3.1. Energy levels and wavelengths

In Table 2 we compare present level energies with experiment and SAF. It may be seen that the energies obtained for the K-vacancy levels with approximation AST1 are on average  $10 \pm 2$  eV higher than experiment. By including the Breit interaction (AST2), and mainly due to the contribution from the non-fine structure two-body terms, this discrepancy is slightly reduced to  $8 \pm 1$  eV. Further consideration of CI, i.e. from configurations of the  $n = 3$  complex, does not bring about noticeable improvements. Results obtained with BPR1 bear a similar degree of discord. This systematic difference is partly due to neglected interactions (e.g. QED), but also to the fact that orthogonal orbital bases are used to represent both the ground and lowly excited bound states, in the one hand, and the highly excited K-vacancy resonances on the other thus discarding core relaxation effects. Since HFR can generate

variationally separate sets of orbitals for each configuration, it leads to more accurate *ab initio* energies: the average discrepancy of HFR1 with experiment is only  $2 \pm 1$  eV. Fine tuning, invoked in approximations AST3 and HFR2, results in theoretical levels within 1 eV of experiment, comparable to the accuracy of 1.5 eV displayed by SAF. For the unobserved  $1s2s2p\ ^4P_{5/2}^o$  level, an energy of  $6.6285(3)$  keV is predicted which is in good accord with value of 6.6283 keV quoted by SAF.

In Table 3 we compare line wavelengths derived from the AST3 and HFR2 approximations with experiment and other theoretical results. The measurements were made by Beiersdorfer et al. (1993) with a high-resolution Bragg crystal spectrometer on the Princeton Large Torus Tokamak. Our previous criticism regarding the incompleteness of the experimental data sets is clearly supported by this comparison. With respect to experiment, differences with HFR2 and SAF are not larger than  $0.4$  mÅ while those with AST3 and MCDF are within  $0.6$  mÅ and  $0.8$  mÅ respectively. This level of accord is somewhat outside of the average experimental precision of  $0.23$  mÅ. The values listed by COR are systematically shorter than experiment by  $\sim 3$  mÅ and the *ab initio* results by BPR2 can be discrepant by a similar amount. In general, differences between the AST3, HFR2, SAF, and MCDF data sets show scatters with standard deviations not larger than  $0.3$  mÅ which can perhaps be taken as a lower bound of theoretical accuracy.

### 3.2. Radiative rates

A Li-like K-vacancy state decays radiatively by emitting a  $K\alpha$  photon:

$$1s2s^{n_k}2p^{m_k}\ ^{(2S_k+1)}L_{J_k} \rightarrow 1s^22l_i\ ^2L'_{J_i} + \gamma. \quad (15)$$

The strong transitions are the dipole spin-allowed ( $2S_k + 1 = 2$ ) but intercombination transitions ( $2S_k + 1 = 4$ ) can also take place through subtle relativistic couplings. Furthermore, we have found that in some cases the forbidden transitions must also be considered.

In Table 4 we present transition probabilities computed in the different approximations together with those from previous work: BPR2, COR, SAF, and MCDF. In the following discussion, we exclude the transitions 10–3, 12–1, 13–2, and 18–2 as they are severely affected by cancellation and nothing further can be asserted about their radiative properties. In Fig. 1 we compare  $A$ -values computed in AST2 with those in AST1 where significant differences are found. In general, the inclusion of the Breit interaction (AST2) increases rates; while the variations are not larger than 10% for the spin allowed transitions that exhibit large rates ( $\log A_r > 14$ ), the enhancement in the intersystem transitions (5–1, 6–1, and 13–3) can be as large as 25%. Inclusion of CI from the  $n = 3$  complex leads to changes not larger

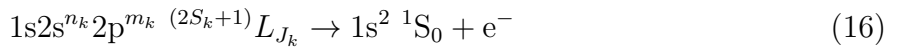
than 2% while the fitting with TEC, as expected, causes differences mostly in the sensitive intersystem transitions.

In Fig. 2a the transition probabilities computed in approximation AST1 are compared with those by HFR1, COR, SAF, and MCDF. While there is excellent agreement with COR (within 10%), the data in HFR1 and SAF are on average higher by  $\sim 5\%$  with scatters of  $\pm 4\%$  and  $\pm 12\%$ , respectively. Differences with MCDF are as large as 21%. It can be inferred from this comparison that COR most probably did not consider the relativistic two-body corrections, and the discord with HFR1, SAF, and MCDF is mostly due to the contributions from these operators. This assertion is supported by a further comparison with the data in AST3 (Fig. 2b); now the agreement with SAF and MCDF has improved to  $\sim 10\%$  while discrepancies as large as 25% are found with COR. The larger differences now found with HFR2 (15%) are an indication that the Blume–Watson screening in HFR does not account adequately for the Breit interaction. The outcome of this comparison clearly brings out the relevance of the latter in the radiative decay, and give us confidence on the accuracy ranking (better than 10%) that can be assigned to the  $A$ -values in AST3 and on the reliability of AUTOSTRUCTURE platform in the study of the decay properties of K-vacancy states.

We have found that the K-vacancy states in Li-like iron, in addition to their dipole allowed manifold, can also decay radiatively via unusually strong magnetic transitions. As shown in Table 5, the  $A$ -values for the M2 components in 10–3 and 13–2 are almost as large as their E1 counterparts, and therefore must be taken into account in order to maintain accuracy. The situation becomes critical for the  $1s2s2p\ ^4P_{5/2}^o$  metastable which is shown to decay through both M1 and M2 transitions (see Table 5). It may be also appreciated that the M1  $A$ -value must be calculated with the relativistically corrected operator (see Eq. 9) since the difference with the uncorrected version is 5 orders of magnitude. Chen et al. (1981) have assumed that this state decays radiatively only via the M2 transition, and quote a value of  $A_r = 6.57 \times 10^9 \text{ s}^{-1}$  in good agreement (7%) with the present  $A_{M2}$ -value of  $6.16 \times 10^9 \text{ s}^{-1}$ .

### 3.3. Auger rates

While the radiative transition probabilities can be resolved satisfactorily, the effects of the magnetic couplings on the Auger rates are more evident and thus larger the discrepancies. A Li-like K-vacancy level autoionizes through the single channel



that ends up in the ground state of the He-like child ion. A comparison of rates is given in Table 6. As before, due to strong cancellation effects, we exclude the  $1s(^2S)2s2p(^3P^o) \ ^2P_{3/2}^o$

and  ${}^4P_{1/2}^o$  states from further discussion. By comparing data from approximations AST1 and AST2 (see Fig. 3), it is found significant sensitivity to the Breit interaction: states with  $\log A_a > 13$  are in general reduced by no more than 11%, but the smaller values show decrements as large as a factor of 2. In this respect and as shown in Table 7, the spin–spin interaction can cause drastic changes in the rates, not only due to level coupling within the parent bound configurations (bound–bound coupling) but also involving the final continuum configuration (bound–free coupling). An outstanding illustration of this correlation is the  $1s2s2p\ {}^4P_{5/2}^o$  state which can only autoionize through the spin–spin interaction. By contrast, CI from the  $n = 3$  complex is found to be relatively unimportant, but the TEC lead to noticeable changes (25%) in the quartet states, e.g.  $1s2p^2\ {}^4P_J$ , that can only decay through relativistic intersystem couplings that are sensitive to level separation. The good agreement ( $\sim 10\%$ ) between AST1 and BPR1 for states with  $\log A_a > 13$  reinforces the AUTOSTRUCTURE numerical formulation of autoionization processes, and that between BPR1 and BPR2, further confirmation that CI from  $n > 2$  complexes is irrelevant in the decay of K-vacancy states of this ion.

Unexpected large discrepancies are encountered with the data computed with the HFR code. In the case of HFR3, they can perhaps be attributed to the simple atomic model adopted by Lemen et al. (1984) that neglects both CI and the Breit interaction, but their origin in HFR1 and HFR2 are less clear. Taking into consideration that we have computed reliable Auger rates for other Fe ions with this code, the cause could be tentatively ascribed to an oversimplified implementation of the Breit interaction.

In Fig. 4 Auger rates in AST1 and AST3 are compared with COR, SAF, and MCDF. While agreement between COR and AST1 is within 10%, it clearly deteriorates with AST3; this is further evidence of the neglect of the Breit interaction by COR. Significant differences are also found with SAF and MCDF in particular for the smaller values ( $\log A_a < 13$ ). Focusing our discussion on the larger rates, data by SAF are on average 8% higher than AST1 which is a worrying outcome as the inclusion of the Breit interaction in general decreases our rates thus magnifying the discrepancy. This can be appreciated in the comparison of SAF with AST3 in Fig. 4b where the larger differences are found for decays subject to strong spin–spin bound–free correlation (see Table 7), and can perhaps be attributed to its deficient treatment in the SAF approach. By contrast, the discord between AST1 and MCDF for the larger rates (up to 32%) is reduced to within 15% when the Breit interaction is taken into account.

The lack of data stability for Auger transitions with  $\log A_a < 13$  is further put in evidence in the tricky decay of the  $1s2s2p\ {}^4P_{5/2}^o$  state. While there is good agreement with Chen et al. (1981) for the dominant radiative M2  $A$ -value (see Section 3.2), their Auger rate

of  $6.53 \times 10^9 \text{ s}^{-1}$  is a factor of 3 larger thus predicting a lower fluorescence yield (0.50) than the present (0.76) for this state.

### 3.4. $B_r$ and $Q_d$ factors

In the spectral synthesis of dielectronic satellite lines, relevant parameters for a  $k \rightarrow i$  radiative emission are the branching ratio

$$B_r(k, i) \equiv \frac{A_r(k, i)}{A_r(k) + A_a(k)} \quad (17)$$

and the satellite intensity factor

$$Q_d(k, i) \equiv g_k B_r(k, i) A_a(k) \quad (18)$$

where  $A_r(k, i)$ ,  $A_r(k) = \sum_i A_r(k, i)$ ,  $A_a(k)$ , and  $g_k$  are respectively the  $A$ -value, total radiative width, Auger rate and statistical weight of the upper  $k$  level. In Table 8 we compare our best data set (AST3) with COR, SAF, and MCDF. For  $B_r > 0.1$ , the agreement is within 5% except for the COR 13–3 and the SAF 11–1 lines where it deteriorates to 9%. The former, being an intercombination transition, is sensitive to the atomic model while level 11 is subject to admixture. For  $B_r < 0.1$ , the accord is within 15% if transitions affected with cancellation are put aside. For  $Q_d > 10^{13} \text{ s}^{-1}$ , agreement with COR, SAF, and MCDF is respectively within 10%, 25%, and 15%, but for the smaller values, discrepancies up to a factor of 9 do appear.

## 4. Summary and conclusions

As a starting point in a project to compute improved atomic data for the spectral modeling of Fe K lines, we have carried out extensive calculations and comparisons of  $A$ -values and Auger rates for the K-vacancy states of the Li-like Fe XXIV system. Primary aims have been to select an applicable computational platform and an efficient strategy to generate accurate and complete data sets for other members of the first row of the Fe isonuclear sequence.

Several physical effects have been considered: orbital representations, CI, relativistic corrections, cancellation, and semi-empirical improvements. For an  $N$ -electron ion, we have found that the most realistic representation is to have different orbital representations for the K-vacancy resonances and the valence states. This is currently available in the HFR code, but most other platforms use orthogonal orbital bases for computational efficiency. In the

case of AUTOSTRUCTURE, which uses a pseudo-continuum approach to compute Auger rates, orbitals of the  $(N - 1)$ -electron system must then be used. Level couplings within the  $n = 2$  complex have been found to be vital thus seriously questioning the reliability of the atomic model adopted by Lemen et al. (1984). CI from higher complexes contributes negligibly. The two-body relativistic operators, both fine structure and non-fine structure, play conspicuous roles in the decay pathways of the K-vacancy states of this ion, particularly in the Auger processes. Electron correlation could be then interpreted as being highly magnetic: both bound–bound and bound–free spin–spin couplings have been shown to be large within the  $n = 2$  complex and specially critical in the Auger decay of the  $1s2s2p\ ^4P_{5/2}^0$  state. This state is also shown to decay radiatively through forbidden M1 and M2 transitions, the former requiring a relativistic corrected transition operator to avoid errors in the line strength of several orders of magnitude. In this highly ionized magnetic scenario, computer programs that do not include a formal numerical implementation of the Breit interaction, or neglect it, have limited applicability. Such is the case of BPRM and HFR. We have also looked into cancellation effects, finding several transitions with acute disorders that discourage any discussion about their properties. TEC have been found to be a useful option to attain high numerical accuracy, specially for line identification and to render intersystem couplings that can be sensitive to level splittings.

In the light of the problems discussed above, AUTOSTRUCTURE emerges as the platform of choice. This implies that the present calculation ends up being an independent validation of the work by COR and, by including improved magnetic correlations and fine tuning, a substantial refinement. The level of agreement found with COR at the different stages of the present comparisons confirms this assertion. The excellent accord also obtained with the radiative rates by SAF and MCDF allow us to establish a firm ranking of better than 10% for the AST3  $A$ -values. On the other hand, the fairly large discrepancies with the SAF Auger rates are believed to be caused by their rough treatment of the Breit interaction in terms of screening constants. From the agreement with MCDF, on the other hand, the present autoionization data with  $\log A_a > 13$  can be ranked to within 15%. We can also conclude from the comparison with SAF that the precision attained for the K-vacancy level energies of  $\pm 1$  eV is a lower bound of present computational capabilities. Since it necessarily relies on fine tuning, and considering the current unavailability of complete experimental K-vacancy level structures for Fe ions, further spectroscopic data would be an asset.

The present methodology of using several computational platforms to treat inner-shell processes has proven to be key in elucidating the physics involved and the level of accuracy. It was previously exploited by COR and SAF and more recently by Savin et al. (2002), and it will be therefore maintained in our calculations on other members of the Fe isonuclear sequence.

We are indebted to Dr. Nigel Badnell (University of Strathclyde, UK) for invaluable discussions regarding the AUTOSTRUCTURE options and Auger processes in general, and to Dr. Claude Zeippen (Observatoire de Paris, France) for assistance with the relativistic corrections of the M1 operator. CM acknowledges a Senior Research Associateship from the National Research Council.

## REFERENCES

Badnell, N. R. 1986, J. Phys. B 19, 3827

Badnell, N. R. 1997, J. Phys. B 30, 1

Bautista, M.A., Kallman, T.R. 2000, ApJ 544, 581

Beiersdorfer, P., Phillips, T., Jacobs, V. L., et al. 1993, ApJ 409, 846

Beiersdorfer, P., Bitter, M., von Goeler, S., Hill, K. W. 1989, Phys. Rev. A 40, 150

Berrington, K. A., Burke, P. G., Butler, K., et al. 1987, J. Phys. B 20, 6379

Berrington, K. A., Burke, P. G., Chang, J. J., et al. 1974, Comput. Phys. Commun. 8, 149

Berrington, K. A., Burke, P. G., Le Dourneuf, M., et al. 1978, Comput. Phys. Commun. 14, 367

Burke, P. G., Hibbert, A., Robb, W.D. 1971, J. Phys. B 4, 153

Burke, P. G., Seaton, M. J. 1971, Meth. Comp. Phys. 10, 1

Chen M. H. 1986, At. Data Nucl. Data Tables 34, 301

Chen M. H., Crasemann, B., Mark, H. 1981, Phys. Rev. A 24, 1852

Chubb, T. A., Friedman, H., Kreplin, R. W. 1963, AJ 68, 277

Cowan, R. D. 1981, *The Theory of Atomic Structure and Spectra* (Berkeley, CA: University of California Press)

Decaux, V., Beiersdorfer, P. 1993, Phys. Scr T47, 80

Decaux, V., Beiersdorfer, P., Kahn, S. M., Jacobs, V. L. 1997, ApJ 482, 1076

Decaux, V., Beiersdorfer, P., Osterheld, A., et al. 1995, ApJ 443, 464

Doschek, G. A., Feldman, U., Cowan, R. D. 1981, ApJ 245, 315

Drake, G. W. F. 1971, Phys. Rev. A 3, 908

Dubau, J., Loulergue, M. 1981, Phys. Scr 23, 136

Eissner, W., Jones, M., Nussbaumer, H. 1974 Comput. Phys. Commun. 8, 270

Eissner, W., Nussbaumer, H. 1969, J. Phys. B 2, 1028

Eissner, W., Zeippen, C. J. 1981, J. Phys. B 14, 2125

Jacobs, V. L., Rozsnyai, B. F. 1986 Phys. Rev. A 34, 216

Jacobs, V. L., Davis, J., Rosznyai, B. F., Cooper, J. W. 1980 Phys. Rev. A 21, 1917

Kato, T., Safranova, U. I., Shlyaptseva, A. S., et al. 1997, At. Data Nucl. Data Tables 67, 225

Lemen, J. R., Phillips, K. J. H., Cowan, R. D., et al. 1984, A&A 135, 313

Nahar, S. N., Pradhan, A. K., Zhang, H. L. 2002, Phys. Rev. A 63, 060701 (R)

Oelgoetz, J., Pradhan, A.K. 2001, MNRAS 327, L42

Pravdo, S.H., Becker, R.H., Boldt, E.A., et al. 1977, ApJ 215, L61

Quigley, L., Berrington, K. 1996, J. Phys. B 29, 4529

Quigley, L., Berrington, K., Pelan, J. 1998, Comput. Phys. Commun. 114, 225

Safranova, U. I., Shlyaptseva, A. S. 1996, Phys. Scr 54, 254

Sanford, P., Mason, K.O., Ives, J., 1975, MNRAS 173, 9P

Savin, D. W., Behar, E., Kahn, S. M., et al. 2002, ApJS 138, 337

Scott. N. S., Burke, P. G. 1980, J. Phys. B 13, 4299

Scott. N. S., Taylor, K. T. 1982, Comput. Phys. Commun. 25, 347

Seely, J. F., Feldman, U., Safranova, U. I. 1986, ApJ 304, 838

Serlemitsos, P.J., Boldt, E.A., Holt, S.S., et al. 1973, ApJ 184, L1

Serlemitsos, P.J., Smith, B.W., Boldt, E.A., et al. 1977, ApJ 211, L63

Shirai, T., Sugar, J., Musgrove, A., Wiese, W. L. 2000, J. Phys. Chem. Ref. Data, Monograph 8

Tanaka, Y., Nandra, K., Fabian, A. C., et al. 1995, Nature 375, 659

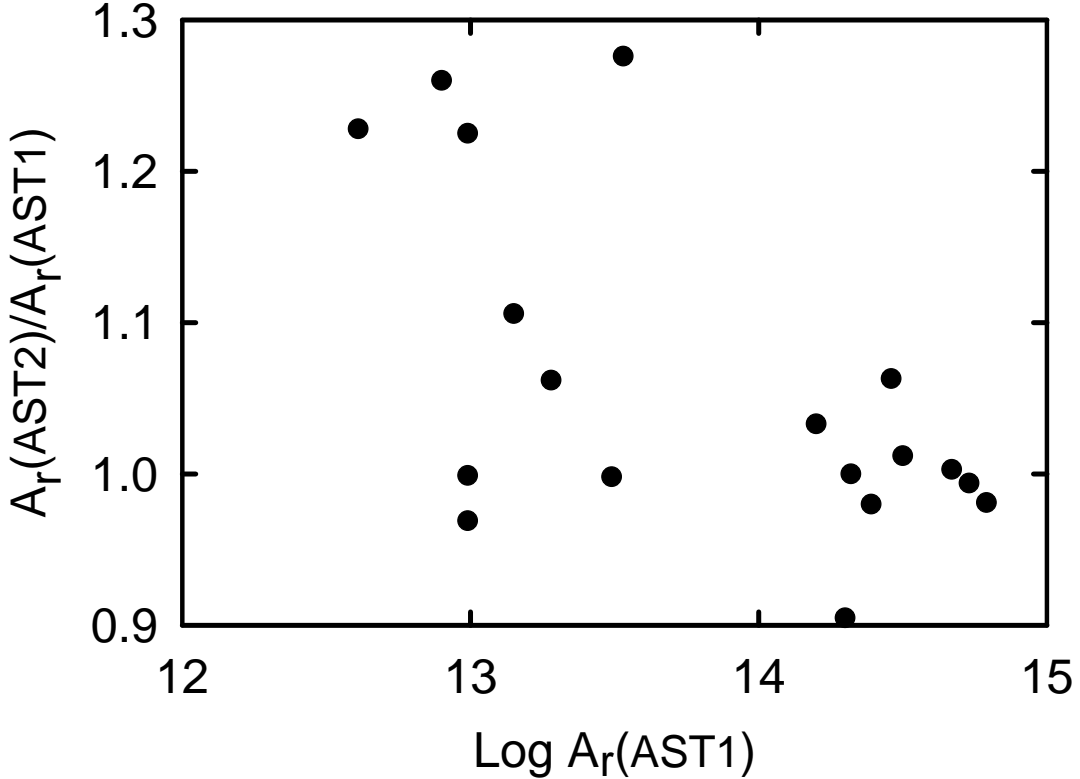


Fig. 1.— Comparison of  $A$ -values ( $s^{-1}$ ) for K transitions in Fe XXIV computed with approximations AST1 and AST2. Differences are due to Breit interaction.

Table 1. Approximation key

Feature	AST1	AST2	AST3	HFR1	HFR2	HFR3	BPR1	BPR2	COR	SAF	MCDF
Orthogonal orbital basis	Yes	Yes	Yes	No	No	No	Yes	Yes	Yes	Yes	Yes
CI from $n > 2$ complexes	No	No	Yes	No	Yes	No	No	Yes	?	Yes	Yes
Breit interaction	No	Yes	Yes	Yes	Yes	No	No	?	Yes	Yes	
QED effects	No	Yes	Yes	Yes							
Semi-empirical corrections	No	No	Yes	No	Yes	No	No	No	No	No	No

References. — AST1–AST3: Present work (AUTOSTRUCTURE). HFR1–HFR2: Present work (HFR). HFR3: HFR calculation by Lemen et al. (1984). BPR1: Present work (BPRM). BPR2: BPRM calculation by Nahar et al. (2002). COR: Cornille data set from Kato et al. (1997). SAF: Safranova data set from Kato et al. (1997) and Safranova & Shlyaptseva (1996). MCDF: Multiconfiguration Dirac–Fock calculation by Chen (1986).

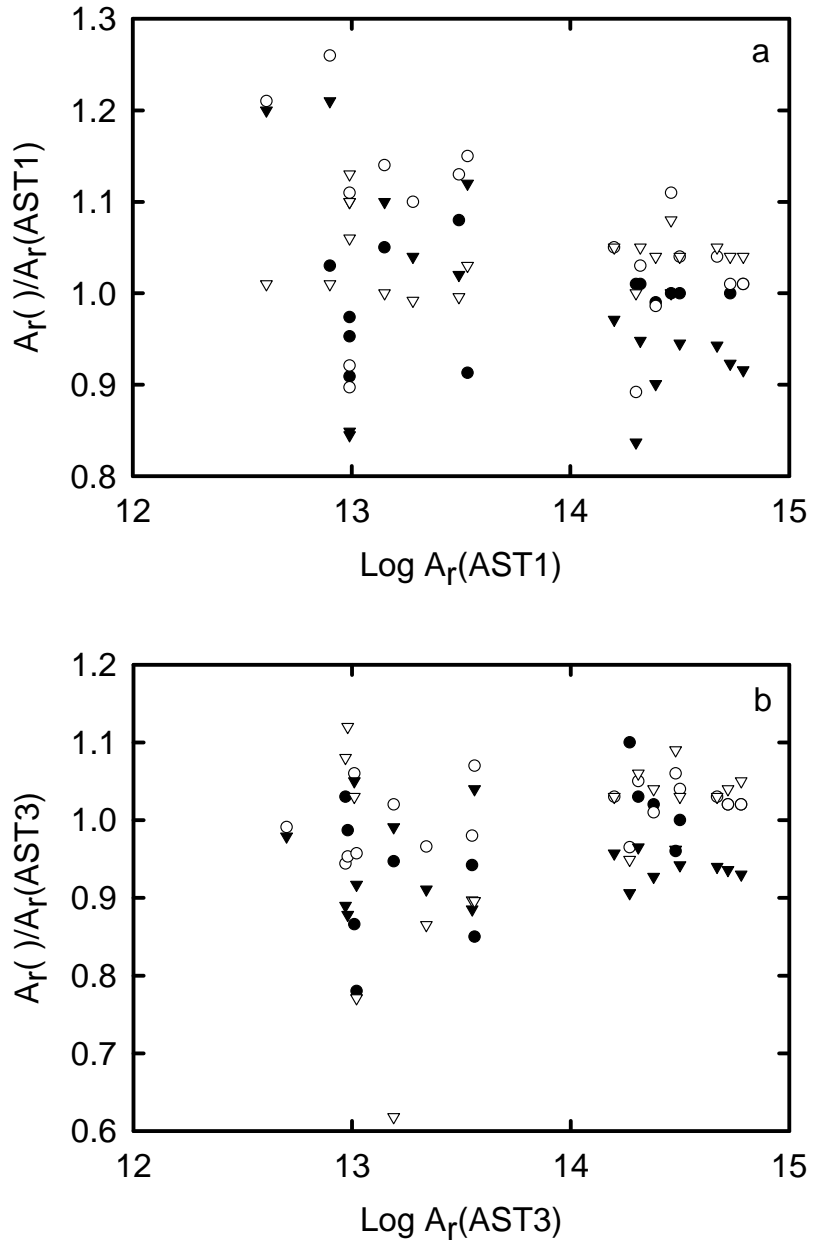


Fig. 2.— Comparison of AUTOSTRUCTURE  $A$ -values ( $s^{-1}$ ) for K transitions in Fe xxiv with other approximations and external data sets. (a) AST1 with: HFR1 (triangles); COR (filled circles); SAF (circles); and MCDF (filled triangles). (b) AST3 with: HFR2 (triangles); COR (filled circles); SAF (circles); and MCDF (filled triangles).

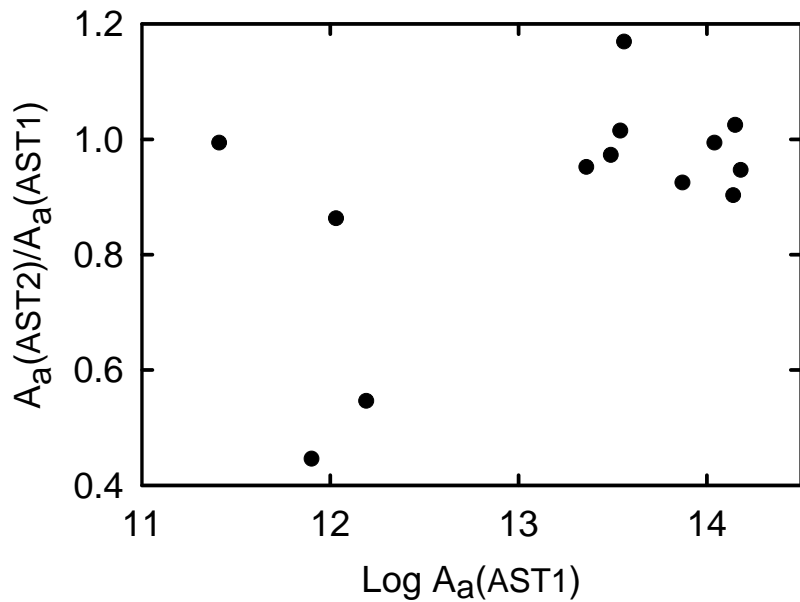


Fig. 3.— Comparison of Auger rates ( $\text{s}^{-1}$ ) for K-vacancy levels of Fe XXIV computed with approximations AST1 and AST2. Differences are due to Breit interaction.

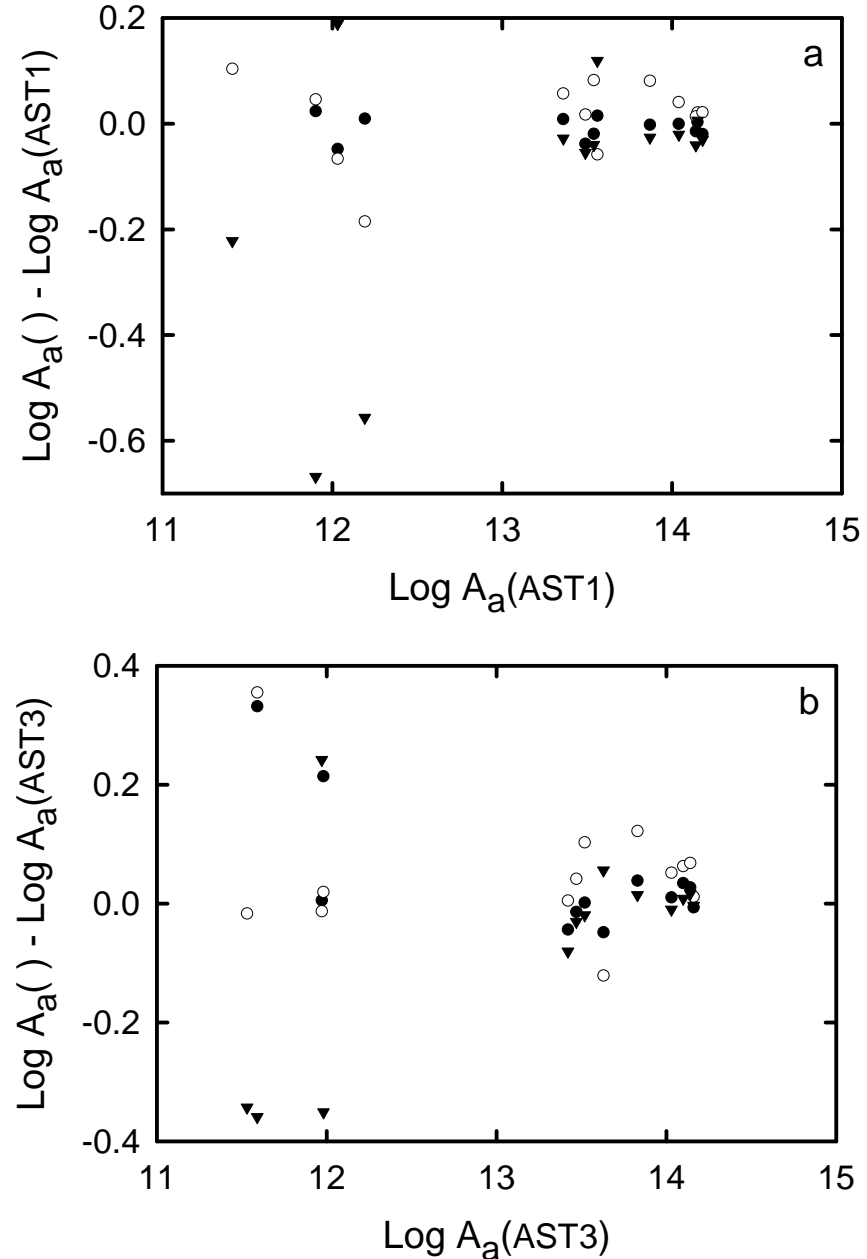


Fig. 4.— Comparison of AUTOSTRUCTURE Auger rates ( $\text{s}^{-1}$ ) for K-vacancy levels in Fe XXIV with previous data sets. (a) AST1 with: COR (filled circles); SAF (circles); and MCDF (filled triangles). (b) AST3 with: COR (filled circles); SAF (circles); and MCDF (filled triangles).

Table 2. Level energies (keV) for the  $n = 2$  complex of Fe XXIV

<i>i</i>	State	Expt <sup>a</sup>	AST1	AST2	AST3	HFR1	HFR2	BPR1	BPR2	SAF
1	$1s^2 2s\ 2S_{1/2}$	0.0	0.0	0.0	0.0	0.0	0.0	0.0	0.0	0.0
2	$1s^2 2p\ 2P_{1/2}^o$	0.048600	0.048011	0.049282	0.047778	0.048499	0.048599			0.048540
3	$1s^2 2p\ 2P_{3/2}^o$	0.064566	0.066960	0.066885	0.064975	0.064539	0.064566			0.064534
4	$1s 2s^2\ 2S_{1/2}$	6.6004	6.6099	6.6070	6.6003	6.6018	6.6004	6.6072		6.6011
5	$1s(^2S)2s2p(^3P^o)\ 4P_{1/2}^o$	6.6137	6.6202	6.6189	6.6131	6.6129	6.6131	6.6177	6.617	6.6135
6	$1s(^2S)2s2p(^3P^o)\ 4P_{3/2}^o$	6.6167	6.6253	6.6227	6.6169	6.6178	6.6173	6.6230	6.627	6.6171
7	$1s(^2S)2s2p(^3P^o)\ 4P_{5/2}^o$		6.6376	6.6342	6.6285	6.6295	6.6265			6.6283
8	$1s(^2S)2s2p(^3P^o)\ 2P_{1/2}^o$	6.6535	6.6624	6.6598	6.6525	6.6538	6.6537	6.6605	6.649	6.6534
9	$1s(^2S)2s2p(^3P^o)\ 2P_{3/2}^o$	6.6619	6.6732	6.6697	6.6623	6.6641	6.6618	6.6708	6.663	6.6624
10	$1s(^2S)2p^2(^3P)\ 4P_{1/2}$	6.6710	6.6781	6.6770	6.6706	6.6709	6.6708	6.6764		6.6717
11	$1s(^2S)2s2p(^1P^o)\ 2P_{1/2}^o$	6.6764	6.6866	6.6841	6.6764	6.6784	6.6766	6.6831	6.674	6.6765
12	$1s(^2S)2s2p(^1P^o)\ 2P_{3/2}^o$	6.6792	6.6896	6.6867	6.6791	6.6812	6.6790	6.6869	6.681	6.6795
13	$1s(^2S)2p^2(^3P)\ 4P_{3/2}$	6.6793	6.6868	6.6855	6.6792	6.6790	6.6786	6.6853		6.6798
14	$1s(^2S)2p^2(^3P)\ 4P_{5/2}$	6.6850	6.6946	6.6917	6.6850	6.6865	6.6857	6.6932		6.6856
15	$1s(^2S)2p^2(^1D)\ 2D_{3/2}$	6.7027	6.7137	6.7118	6.7027	6.7050	6.7029	6.7112		6.7042
16	$1s(^2S)2p^2(^3P)\ 2P_{1/2}$	6.7046	6.7159	6.7128	6.7041	6.7068	6.7048	6.7141		6.7052
17	$1s(^2S)2p^2(^1D)\ 2D_{5/2}$	6.7090	6.7211	6.7176	6.7089	6.7120	6.7096	6.7189		6.7097
18	$1s(^2S)2p^2(^3P)\ 2P_{3/2}$	6.7224	6.7349	6.7315	6.7225	6.7247	6.7219	6.7329		6.7230
19	$1s(^2S)2p^2(^1S)\ 2S_{1/2}$	6.7415	6.7541	6.7514	6.7414	6.7448	6.7412	6.7519		6.7428

<sup>a</sup>Experimental level energies from Shirai et al. (2000).

Table 3. Wavelengths ( $\text{\AA}$ ) for K transitions in Fe XXIV

Label <sup>a</sup>	<i>k</i>	<i>i</i>	Expt <sup>b</sup>	AST3	HFR2	COR	SAF	MCDF	BPR2
p	4	2	1.89219(25)	1.8922	1.8924	1.8894	1.8924	1.8927	
o	4	3	1.89680(20)	1.8971	1.8970	1.8946	1.8969	1.8973	
v	5	1		1.8748	1.8748		1.8748	1.8752	1.873
u	6	1	1.87347(35)	1.8737	1.8736	1.8712	1.8738	1.8742	1.870
	7	1		1.8706					
	7	3		1.8890					
r	8	1	1.86325(20)	1.8639	1.8634	1.8611	1.8635	1.8640	1.864
q	9	1	1.86104(15)	1.8610	1.8611		1.8610	1.8613	1.860
i	10	2		1.8720	1.8722		1.8722	1.8725	
h	10	3		1.8768	1.8768		1.8766	1.8771	
t	11	1	1.85693(20)	1.8568	1.8570	1.8543	1.8571	1.8571	1.857
s	12	1		1.8563	1.8563	1.8535	1.8563	1.8564	1.855
g	13	2		1.8697	1.8701		1.8699	1.8702	
f	13	3		1.8745	1.8746	1.8724	1.8743	1.8747	
e	14	3	1.87246(35)	1.8729	1.8726	1.8703	1.8727	1.8730	
k	15	2	1.86325(20)	1.8630	1.8632	1.8601	1.8630	1.8631	
l	15	3		1.8677	1.8677	1.8652	1.8674	1.8676	
d	16	2		1.8626	1.8627	1.8594	1.8628	1.8629	
c	16	3		1.8674	1.8672		1.8672	1.8673	
j	17	3	1.86576(12)	1.8661	1.8658	1.8631	1.8659	1.8660	
b	18	2		1.8576	1.8579	1.8542	1.8578	1.8578	
a	18	3	1.86207(30)	1.8623	1.8624	1.8593	1.8622	1.8622	
n	19	2		1.8523	1.8526	1.8488	1.8523	1.8521	
m	19	3	1.85693(20)	1.8570	1.8570	1.8539	1.8566	1.8565	

<sup>a</sup>Transition labels from Seely et al. (1986).

<sup>b</sup>Tokamak measurements (uncertainties in brackets) by Beiersdorfer et al. (1993).

Table 4.  $A$ -values ( $10^{13}$  s $^{-1}$ ) for K transitions in Fe XXIV

Label <sup>a</sup>	$k$	$i$	AST1	AST2	AST3	HFR1	HFR2	BPR2	COR	SAF	MCDF
p	4	2	9.76–1	9.46–1	9.27–1	1.03+0	1.00+0		9.51–1	8.75–1	8.25–1
o	4	3	9.85–1	9.84–1	9.52–1	1.08+0	1.07+0		9.39–1	9.07–1	8.36–1
v	5	1	4.06–1	4.98–1	4.97–1	4.08–1	2.92–1	3.66–1		4.92–1	4.86–1
u	6	1	1.40+0	1.55+0	1.55+0	1.40+0	9.60–1	1.32+0	1.47+0	1.59+0	1.54+0
	7	1	6.18–4	6.18–4	6.16–4						
	7	3	1.93–5	1.94–5	1.94–5						
r	8	1	2.88+1	3.06+1	3.01+1	3.10+1	3.29+1	2.80+1	2.88+1	3.19+1	2.89+1
q	9	1	4.70+1	4.71+1	4.71+1	4.94+1	4.86+1	4.74+1		4.87+1	4.43+1
i	10	2	1.90+0	2.02+0	2.17+0	1.89+0	1.88+0			2.10+0	1.98+0
h	10	3	1.77–2	7.70–3	9.12–3	1.79–2	1.60–2			9.30–3	1.27–2
t	11	1	2.01+1	1.82+1	1.86+1	2.01+1	1.76+1	2.14+1	2.03+1	1.79+1	1.68+1
s	12	1	8.92–1	5.90–1	4.19–1	6.57–1	1.25+0	5.83–1	4.41–1	7.78–2	3.23–1
g	13	2	6.21–2	6.63–3	4.51–3	9.03–3	1.06–2			2.40–3	3.42–3
f	13	3	8.01–1	1.01+0	1.06+0	8.11–1	8.13–1		8.23–1	1.01+0	9.67–1
e	14	3	3.11+0	3.11+0	3.58+0	3.10+0	3.21+0		3.37+0	3.51+0	3.17+0
k	15	2	3.13+1	3.17+1	3.14+1	3.26+1	3.24+1		3.15+1	3.27+1	2.96+1
l	15	3	3.39+0	4.32+0	3.64+0	3.49+0	3.26+0		3.09+0	3.90+0	3.80+0
d	16	2	5.39+1	5.35+1	5.31+1	5.62+1	5.53+1		5.39+1	5.44+1	4.97+1
c	16	3	1.58+1	1.63+1	1.60+1	1.66+1	1.65+1			1.65+1	1.53+1
j	17	3	2.09+1	2.09+1	2.05+1	2.19+1	2.17+1		2.11+1	2.16+1	1.98+1
b	18	2	1.15+0	7.70–1	9.69–1	1.21+0	1.24+0		1.25+0	8.63–1	7.57–1
a	18	3	6.16+1	6.04+1	6.07+1	6.43+1	6.37+1		6.20+1	6.21+1	5.64+1
n	19	2	9.78–1	1.20+0	1.03+0	1.11+0	1.06+0		8.89–1	1.09+0	1.08+0
m	19	3	2.46+1	2.42+1	2.40+1	2.56+1	2.49+1		2.44+1	2.43+1	2.22+1

<sup>a</sup>Transition labels from Seely et al. (1986).

Note. —  $a \pm b \equiv a \times 10^{\pm b}$

Table 5.  $A$ -values ( $10^9$  s $^{-1}$ ) for K transitions with sizable magnetic components

$k$	$i$	E1	M2	M1/M1 <sup>a</sup>
7	1	0.0	6.16+0	0.0
7	3	0.0	0.0	1.94–1/6.11–7
10	3	9.07+1	5.04–1	0.0
13	2	3.99+1	5.19+0	0.0

<sup>a</sup>Computed with uncorrected M1 operator.

Note. — Data computed with approximation AST3.  $a \pm b \equiv a \times 10^{\pm b}$ .

Table 6. Auger rates ( $10^{13}$  s $^{-1}$ ) for K-vacancy states in Fe xxiv

$i$	AST1	AST2	AST3	HFR1	HFR2	HFR3	BPR1	BPR2	COR	SAF	MCDF
4	1.40+1	1.44+1	1.43+1	8.61+0	8.60+0		1.45+1		1.41+1	1.47+1	1.42+1
5	1.88–2	1.45–3	1.33–3	1.54–2	1.09–2	1.44–2	1.57–2	1.54–2		1.19–2	5.57–3
6	7.96–2	3.55–2	3.91–2	6.56–2	4.31–2	6.39–2	7.07–2	6.45–2	8.40–2	8.85–2	1.71–2
7	0.00+0	1.99–4	1.97–4	0.00+0	0.00+0		0.00+0				
8	3.67+0	4.29+0	4.24+0	3.42+0	2.92+0	2.86+0	3.87+0	3.90+0	3.80+0	3.21+0	4.83+0
9	8.99–4	2.34–2	1.41–2	3.01–2	8.57–2	6.20–3	1.55–2	1.86–2		3.02–2	5.74–2
10	2.55–2	2.53–2	3.37–2	2.21–1	2.23–1	3.46–1	3.15–2			3.24–2	1.53–2
11	7.43+0	6.87+0	6.77+0	7.16+0	7.55+0	5.12+0	7.74+0	7.10+0	7.40+0	8.96+0	7.00+0
12	1.10+1	1.10+1	1.07+1	1.05+1	1.04+1	7.92+0	1.11+1	1.06+1	1.10+1	1.21+1	1.05+1
13	1.55–1	8.44–2	9.66–2	1.37–1	1.42–1	1.17–1	1.78–1		1.58–1	1.01–1	4.30–2
14	2.31+0	2.20+0	2.61+0	2.05+0	2.13+0	1.83+0	2.56+0		2.36+0	2.64+0	2.17+0
15	1.39+1	1.26+1	1.25+1	1.29+1	1.30+1	9.20+0	1.38+1		1.35+1	1.44+1	1.27+1
16	1.06–1	9.16–2	9.39–2	2.58–1	2.55–1	3.68–1	7.01–2		9.50–2	9.08–2	1.64–1
17	1.52+1	1.44+1	1.37+1	1.44+1	1.43+1	1.01+1	1.47+1		1.46+1	1.60+1	1.42+1
18	3.44+0	3.49+0	3.28+0	3.37+0	3.29+0	2.57+0	3.19+0		3.29+0	4.16+0	3.14+0
19	3.09+0	3.00+0	2.92+0	5.86+0	5.86+0	4.24+0	2.75+0		2.83+0	3.21+0	2.72+0

Note. —  $a \pm b \equiv a \times 10^{\pm b}$

Table 7. Spin-spin contribution to Auger rates ( $10^{13}$  s $^{-1}$ )

<i>i</i>	AST1	AST1+SS <sup>a</sup>	AST1+SS <sup>b</sup>
4	1.40+1	1.31+1	1.40+1
5	1.88-2	3.70-3	3.42-3
6	7.96-2	4.27-2	2.96-2
7	0.0	0.0	1.99-4
8	3.67+0	3.92+0	3.98+0
9	8.99-4	1.61-1	4.24-3
10	2.55-2	2.11-2	2.69-2
11	7.43+0	6.47+0	7.52+0
12	1.10+1	1.02+1	1.09+1
13	1.55-1	7.99-2	3.82-2
14	2.31+0	2.00+0	2.06+0
15	1.39+1	1.14+1	1.41+1
16	1.06-1	7.37-2	1.01-1
17	1.52+1	1.29+1	1.57+1
18	3.44+0	3.42+0	3.11+0
19	3.09+0	2.67+0	3.09+0

<sup>a</sup>Bound-free spin-spin coupling neglected.

<sup>b</sup>Bound-free spin-spin coupling included.

Note. —  $a \pm b \equiv a \times 10^{\pm b}$

Table 8. Radiative branching ratios  $B_r$  and satellite intensity  $Q_d$  factors

Label <sup>a</sup>	<i>k</i>	<i>i</i>	AST3		COR		SAF		MCDF	
			$B_r(k, i)$	$Q_d(k, i)$ ( $10^{13} \text{ s}^{-1}$ )	$B_r(k, i)$	$Q_d(k, i)$ ( $10^{13} \text{ s}^{-1}$ )	$B_r(k, i)$	$Q_d(k, i)$ ( $10^{13} \text{ s}^{-1}$ )	$B_r(k, i)$	$Q_d(k, i)$ ( $10^{13} \text{ s}^{-1}$ )
p	4	2	5.72–2	1.64+0	6.00–2	1.68+0	5.29–2	1.56+0	5.20–2	1.48+0
o	4	3	5.88–2	1.68+0	5.90–2	1.66+0	5.49–2	1.62+0	5.25–2	1.50+0
v	5	1	9.97–1	2.66–3			9.76–1	2.32–2	9.90–1	1.10–2
u	6	1	9.75–1	1.53–1	9.46–1	3.17–1	9.47–1	3.35–1	9.90–1	6.78–2
	7	1	7.40–1	8.76–4						
	7	3	2.32–2	2.75–5						
r	8	1	8.76–1	7.44+0	8.83–1	6.72+0	9.09–1	5.83+0	8.55–1	8.28+0
q	9	1	1.00+0	5.64–2			9.99–1	1.21–1	9.98–1	2.29–1
i	10	2	9.81–1	6.61–2			9.81–1	6.35–2	9.85–1	3.01–2
h	10	3	4.12–3	2.77–4			4.35–3	2.82–4	6.30–3	1.93–4
t	11	1	7.33–1	9.92+0	7.33–1	1.08+1	6.67–1	1.19+1	7.05–1	9.88+0
s	12	1	3.76–2	1.61+0	3.80–2	1.70+0	6.41–3	3.09–1	3.00–2	1.25+0
g	13	2	3.90–3	1.51–3			2.16–3	8.72–4	3.38–3	5.81–4
f	13	3	9.13–1	3.53–1	8.27–1	5.23–1	9.07–1	3.67–1	9.53–1	1.64–1
e	14	3	5.78–1	9.06+0	5.88–1	8.34+0	5.71–1	9.04+0	5.93–1	7.72+0
k	15	2	6.61–1	3.29+1	6.55–1	3.53+1	6.41–1	3.70+1	6.43–1	3.25+1
l	15	3	7.66–2	3.82+0	6.40–2	3.47+0	7.64–2	4.41+0	8.25–2	4.18+0
d	16	2	7.68–1	1.44–1	7.72–1	1.47–1	7.67–1	1.39–1	7.65–1	2.51–1
c	16	3	2.31–1	4.34–2			2.32–1	4.21–2	2.35–1	7.70–2
j	17	3	6.00–1	4.92+1	5.92–1	5.17+1	5.73–1	5.52+1	5.83–1	4.95+1
b	18	2	1.49–2	1.96–1	1.90–2	2.47–1	1.29–2	2.14–1	1.26–2	1.58–1
a	18	3	9.35–1	1.23+1	9.31–1	1.23+1	9.25–1	1.54+1	9.35–1	1.18+1
n	19	2	3.68–2	2.15–1	3.20–2	1.79–1	3.82–2	2.45–1	4.16–2	2.26–1
m	19	3	8.59–1	5.01+0	8.67–1	4.90+0	8.50–1	5.46+0	8.55–1	4.64+0

<sup>a</sup>Transition labels from Seely et al. (1986).

Note. —  $a \pm b \equiv a \times 10^{\pm b}$